X-Ray Imaging of Immiscible Fluid Fingering Patterns in a Natural High Porosity Rock

Cyrille Couture, Athanasios Papazoglou, Alessandro Tengattini, Pierre Bésuelle, Gioacchino Viggiani

frontiers

X-ray imaging of immiscible fluid fingering patterns in a natural high porosity rock

Cyrille Couture [1,2,*], **Athanasios Papazoglou** [3], **Alessandro Tengattini** [1,2], **Pierre Bésuelle** [1] **and Gioacchino Viggiani** [1]

[1] *Univ. Grenoble Alpes, CNRS, Grenoble INP, 3SR, Grenoble, France*
[2] *Institute Laue-Langevin, Grenoble, France*
[3] *Novitom, Grenoble, France*

Correspondence*:
Cyrille Couture
cyrille.couture@3sr-grenoble.fr

ABSTRACT

This paper presents the development of a laboratory scale apparatus and first experimental results on the characterization of fingering patterns of immiscible fluids in a porous rock (Fontainebleau sandstone), using three dimensional full-field measurements from x-ray tomography. The few existing studies that have extended experimental investigation of immiscible fluid flow from 2D to 3D have been primarily interested in the pore scale or performed on idealized porous media. While the heterogeneities inherent to natural rocks are known to play an important role on subsurface fluid flow regimes, a limited number of studies have approached the problem of characterizing the time resolved 3D multiphase flow in these material, at the mesoscale. The series of experiments reported in this paper has been performed at a low viscosity ratio, water invasion into oil as the defending fluid, and different capillary numbers (1.8 orders of magnitude). The results illustrate the qualitative transition in the flow regime, from capillary fingering to viscous fingering. While a full quantitative characterization the geometrical features of the fingers will require further technical refinements, a qualitative understanding can be already gathered from the results presented herein.

Keywords: immiscible fluids, x-ray tomography, viscous fingering, capillary fingering, flow instability

1 INTRODUCTION

The study of immiscible fluid flow in porous media is of great scientific interest to assess fluid migration in geological repositories such as sedimentary rock reservoirs. The interaction between the intrinsically heterogeneous porous structure of the host material and the interface between percolating fluids plays an important role in the possible development of unstable flow patterns, giving rise to localized favourable flow paths and entrapment clusters at the mesoscale. The natural occurrence of immiscible fluid interactions in oil-water reservoirs, as well as artificial injections of non-native fluids (e.g., multiphase carbon dioxide and water, hydrogen and water) for recovery and storage, has led to an increasing amount of research aimed at characterizing the site conditions which favours or prevent the development of unstable fluid fronts and residual entrapment.

At the scale of the porous network, the study of immiscible fluid flow instabilities in laboratory settings has been facilitated by the development of experimental systems combining fluid percolation cells and full-field measurement techniques. Such apparatus were initially extended, with the addition of a solid porous phase, to Hele-Shaw cells (Hele-Shaw, 1898), which were previously used to study 2D multiphase flow between two parallel plates (e.g. Paterson, 1981). In a seminal work in the field, Lenormand and Zarcone (1985) proposed a new method to characterize multiphase flow inside idealized 2D porous media, using series of optical images acquired during the invasion process. Shortly after, in an extensive experimental and numerical study, Lenormand et al. (1988) proposed that the spatial distribution of immiscible fluid pairs during the invasion process in a 2D porous medium is primarily controlled by two dimensionless numbers: the viscosity ratio $M = \mu_i/\mu_d$, where μ_i and μ_d are the dynamic viscosity of the invading and defending fluids, respectively, and the capillary number $Ca = \mu_i \nu_i/\sigma$, where ν_i is the velocity of the invading fluid and σ is the interfacial tension. Using the combination of these two dimensionless numbers during different invasion percolation experiments, the authors identified regions in a log $M - Ca$ phase diagram characterizing three main limit flow regimes: (1) stable front displacement, (2) capillary fingering, and (3) viscous fingering. This diagram, with the identified flow regimes and transition regions, is represented in Figure 1. Using similar Hele-Shaw type experimental set-ups (in 2D), subsequent experimental campaigns have also identified the mechanisms behind the unstable flow regimes in idealized porous media (Khosravian et al., 2015; Zhao et al., 2016), comparisons with Saffman-Taylor theoretical solutions (Toussaint et al., 2005), fractal dimension analysis (Lenormand and Zarcone, 1985; Måløy et al., 1985), as well as pore-continuum upscaling relations (Løvoll et al., 2011).

The generalization of flow patterns from idealized 2D porous media to natural 3D porous rocks is not trivial, as it depends on very different geometrical arrangement of the granular structure and flow connectivity in the pore network. As such, advancements in x-ray computed tomography (CT) provide an interesting avenue for the full-field characterization of multi-phase flow in such complex material. With the ability to track the evolution of the fluid interfaces at resolved time increments and at the pore network resolution, x-ray imaging is an essential advancement for studying flow patterns in 3D experimental setups. Experimental studies using x-ray CT have mainly focused on the role of flow instabilities during the invasion process in relatively small percolation domains for geomaterials (Prodanović et al., 2007; Spurin et al., 2019), as well as glass bead packing (Culligan et al., 2006; Datta et al., 2013; Singh et al., 2017). The high resolution at which full-field images were acquired in these studies have enabled to identify important mechanisms in the fluid flow behavior at the pore scale, as well as the role of the granular media structures in relation to the immiscible fluid interface. This highlighted the development of intermittent pathways, the trapping of viscous phase and the role of fluid wetting in the invasion process. In all these studies, however, the experimental setup, with relatively small percolation domains and regions of interests in the images, does not enable the emergence of observable mesoscale fingers which could be compared to the results previously obtained in experiments with 2D Hele-Shaw cells.

In a unique experimental campaign characterizing 3D mesoscale flow patterns, Hu et al. (2020) studied the effects of different viscosity ratios and capillary numbers on the development of fingering structures in a glass bead packing. In this study, the authors proposed, for the first time, an extension of the Ca-M phase diagram in three dimensions and for a wide range of values, using different fluid pairs and injection rates. While the boundaries of the phase diagram, identifying the three different flow regimes (stable front propagation, capillary fingering and viscous fingering), were found to be in agreement with previously reported 2D studies, the authors also noted a wider transition zone between the different regimes. It was also reported that the fractal analysis for capillary fingering was in agreement with predictions from invasion percolation theory (Dias and Wilkinson, 1986; Feder, 1988). The possibility to extend the findings obtained

for packings of spherical beads to natural geomaterials remains an open question. Recent numerical studies where flow simulations were performed using the pore network geometry of natural rocks indicate that there are noticeable differences in the transition of flow patterns and inhibition of fingering between the case of a homogeneous distribution of porosity and the case of strongly heterogeneous porosity distribution, which is typical of natural geomaterials (Liu et al., 2015; Tsuji et al., 2016). While other important experimental campaigns were performed at larger scales on natural rocks (e.g., Riaz et al., 2007; Perrin and Benson, 2010; Berg et al., 2013), these previous studies were not focused on directly characterizing the development and structure of individual fingers.

This paper presents a laboratory experimental system, which has been specifically designed to study the evolution of immiscible fluid fingering in natural sandstone samples. Specifically, the purpose of this work is to experimentally observe the development of fingering structures, by characterizing their ramification and evolving geometry at different flow regimes. While a full quantitative characterization of these geometrical features will require further technical refinements, a qualitative understanding can be already gathered from the results presented herein. Therefore, the apparatus used for this study is made compatible with x-ray CT imaging at the laboratory scale, over a flow domain which is around two orders of magnitude larger than the average pore diameter of the tested rock specimens. The first observations of fingering structures in high porosity Fontainebleau sandstone specimens, tested at three different capillary numbers, are then presented as a preliminary and first outcome of this study.

2 MATERIALS AND METHODS

2.1 Materials

The natural porous rock specimens used in this study are extracted from a single block of Fontainebleau sandstone from the Paris basin in France. This particular sandstone was selected for its high Quartz content (98%), and therefore its inert chemical properties when interacting with percolating fluids. With a porosity of 21%, the pore network consists of a heterogeneous distribution of cemented grains with a mean grain size of 260μm. Specimens of the raw sandstone material are prepared as 13 mm diameter by 26 mm height cylindrical cores extracted at a single orientation and all from the same region of the initial block.

The two immiscible fluids selected for this study are a high viscosity oil and demineralized water doped with a tracing agent. The oil, Total Azolla ZS 150, is the resident fluid initially saturating the porous medium and therefore acts as the defending fluid during the invasion process. At 20°C it has a dynamic viscosity of 330 mPa·s. To enhance the x-ray attenuation contrast of the invading fluid, a 20% mass ratio of sodium iodide, NaI, is mixed into the demineralized water. At this concentration and a temperature of 20°C, the empirical relation for aqueous solutions developed by Laliberté (2007) suggests a dynamic viscosity of 1.22 mPa·s. Using the pendant drop method for this fluid pair, the interfacial tension is measured experimentally to be 40.7 mN/m (Stauffer, 1965).

2.2 Experimental apparatus and protocol

The experimental device is mainly based on a triaxial apparatus designed to optimize the quality of x-ray CT acquisition under various experimental fluid flow and mechanical stress conditions. It serves in this case as a core holder for the sandstone specimen, which is isolated from the confining chamber by a soft membrane. The internal design of the triaxial cell, with an axial piston passing through it, enables to fully decouple radial and axial stresses. While the current system has been used at relatively low confining pressures (0.7 MPa), the apparatus is designed to sustain up to 30MPa. It is therefore a versatile system

which can extend the scope of this campaign to higher pore pressures and coupled hydro-mechanical experiments. A schematic view of the apparatus, with the fluid flow inlet connected to a high precision syringe pump, is shown in Figure 2.

For the test preparation, the sandstone specimen is first gradually saturated inside a vacuum chamber with oil heated at 50^{o}C to reduce its viscosity and reach a homogeneous saturation level. After 24h inside the vacuum chamber, the lateral side of the cylindrical specimen is then wrapped with a layer of Teflon tape to enhance the smoothness of the contact with the sandstone surface. It is then installed inside an oversized heat shrink membrane pre-installed on the bottom platen of the triaxial cell and filled with oil to avoid air entrapment. The sodium iodide saturated water, filling the syringe pump and tubing connector, is then injected until it reaches the inlet of the bottom porous stone. Afterwards, the top cap is installed and the membrane shrunk to the required size, ensuring a tight fit around the specimen, the porous stones and the stainless steel tubes. The triaxial cell is then closed and the confining chamber is gradually pressurized to 0.7MPa.

Each test starts with the simultaneous initiation of fluid injection, at a prescribed and constant flow rate, and the acquisition of x-ray CT scans. The sodium iodide saturated water therefore initially percolates through the bottom porous stone and reaches the specimen to invade the pore space in an average upward movement. The injection and image acquisition proceeds continuously until a clear percolation path is identified in the sequence of x-ray radiographs and the more attenuating invading fluid is seen to reach the top porous stone. Since the injection rate varies greatly from one experiment to the other, by more than an order of magnitude, a careful calibration of the image acquisition is required.

2.3 X-ray image acquisition

The experimental setup described above is installed inside the x-ray scanner at laboratoire 3SR in Grenoble (Viggiani et al., 2014). The acquisition parameters for this series of experiments were selected to optimize the acquisition time, at a resolution and signal-to-noise ratio allowing a clear segmentation of the different fluid phases. The acquisition rate is three x-ray projections per second for a total of 1200 projections per reconstructed CT scan. At this speed, a tomography can be reconstructed over a 400 second time period for a complete 360°rotation. It is therefore relevant to represent the field measurements as a reconstructed volume when the time scale at which the fluid patterns develop are sufficiently slow compared to the acquisition time. However, at fast injection rates, when the breakthrough occurs at or below the time scale of a single CT scan, the filtered back-projection reconstruction method leads to partial volume effects and streak artifacts. In the present study, due to current limitations of the laboratory x-ray scanner, the data from fast injection experiments are represented as the difference between an instantaneous projection and a reference state at the same angle. Although this representation does not enable a quantitative analysis of the 3D finger geometry, the high contrast of the injected fluid is sufficient to qualitatively assess the shape of the developing fluid flow patterns.

3 RESULTS

In a first set of experiments, a series of three invasion percolation processes have been performed with x-ray imaging. For this series of experiments, with sodium iodide enriched water injected into the defending oil, the log value of the viscosity ratio, log(M), is -2.43. Under these conditions, the three selected injection rates of 0.3, 0.05 and 0.005 ml/min also result in log values of the capillary numbers, log(Ca), of -5.90, -6.67 and -7.67 respectively. These values are represented in the phase diagram of Figure 1, where the three experiments are located in the transition region from capillary fingering, at the slowest injection

rate, to viscous fingering, at the fastest injection rate. In this transition region, the change in capillary number by 1.77 orders of magnitude results in significantly different fluid flow patterns, visible in x-ray radiographs. Figure 3 shows this stark contrast in the x-ray radiographs for an intermediate stage during finger development and at the breakthrough time, i.e., when the injected fluid reaches the specimen outlet. In this representation, the attenuation of the injected fluid is highlighted by subtracting the image at the initial state (attenuation contribution of the apparatus and granular structure).

For the higher capillary number,log(Ca)=-5.90, the invasion process occurs rapidly, at a breakthrough time of 15 seconds, with a low invasion volume of the pore space. In this case, a single finger-like structure appears to develop as the main invasion pathway, at a high aspect ratio extending vertically through the sample with limited secondary invasion pathways visible at the bottom of the sample. While radial expansion of the main finger remains limited, it is visible around specific regions of the main pathway between the pair of radiographs in Figure 3a, indicating secondary radial growth well below the finger tip. However, this radial expansion does not seem to mature into new invasion fronts within the time period before breakthrough. Conversely, for the experiment at log(Ca)=-6.67, the invasion fluid is seen to occupy a larger volume of the pore space, before the breakthrough, which occurs after 10 minutes. In the radiographs, two large fingers connected to the inlet can be seen growing simultaneously in the specimen. Although it is not possible to assess their three dimensional aspects in this representation, a substantially larger radial extension of the fingers along their length is visible, compared to the experiment at the higher capillary number. At the tip of the invasion front, smaller structures of limited vertical length are also observed, suggesting that the advancing front is not a homogeneous compact plume but is rather populated by smaller scale substructures. In the experiment at log(Ca)=-7.67, the invasion process occurs at a much slower rate, as reflected by a breakthrough time of 1.2 hours. The invasion front is seen to propagate as a self-similar structure with both a vertical compact front and a radial expansion around a single finger.

Since the invasion process is much slower during the experiment performed at the lowest capillary number, a series of CT scans could be reconstructed during the development of the fingering pattern. Figure 4 shows a time series, as a function of the breakthrough time t*, during the injection of the invading fluid forming a compact structure. The volume increments between each time step are highlighted in the Figure. Since the increments shown are also spaced in time, it can be seen that the main finger initially grows rapidly from the sample inlet. As the interface between the resident oil and injected water increases and, therefore, the radial flow becomes greater, the vertical growth slows down over time. It is also interesting to note the presence of a constriction near the specimen inlet before an expansion into a larger plume, continuously widening as the front progresses vertically through the sample. A secondary finger can be seen to emerge after the breakthrough occurs.

4 DISCUSSION AND CONCLUSIONS

For the series of three experiments presented in this preliminary study, the flow pattern is seen to be influenced by the capillary number, resulting in a transition in the development of fingering structures.

For the high log(Ca) experiment, the invasion process is dominated by viscous fingering, creating thin and rapidly growing pathway of the invading fluid in the direction parallel to the imposed vertical pressure gradient. The observed features of the finger-like structures, with branches developing at a width approaching the pore size length scale of the studied sandstone, are similar to reported fingers in analog 2D porous media (Lenormand et al., 1988). This particular flow pattern results from the heterogeneities naturally present in randomly organized granular arrangements, determining the length scale of the invasion process (Feder, 1988). This random distribution of pore size and connectivity is also known to promote

a fractal growth of the fingers, compared to an organized distribution over the flow domain (Chen and Wilkinson, 1985). Conversely, the propagation of viscous fingers in natural settings can be altered by sample scale heterogeneities, such as layering and preferential pathways, promoting channeling of the invading fluid (Brock and Orr, 1991; De Wit and Homsy, 1997). In the present study, the relatively homogeneous pore size distribution and the absence of sample scale structural features in the host Fontainebleau sandstone cores suggest that the mechanisms driving finger growth is primarily due to viscous forces and pore scale heterogeneities, promoting possible fractal substructures in secondary branches evidenced by a moderate lateral expansion of the main finger.

For this experiment at the highest capillary number, no evidence of flow intermittency is observed. This contrasts with other studies performed in 3D porous media where multiphase flow is primarily driven by viscous forces (Rücker et al., 2015; Spurin et al., 2019; Hu et al., 2020). The difference might be due to the influence of boundary interactions, between the growing fingers and the membrane, thus limiting the number of connected pores around the main pathway. The geometrical aspects of the pores and pore throats can also influence the probability of snap-off events, where flow intermittency tend to occur between intermediate to small pores (Spurin et al., 2019). It is possible that the pore structure of the rock used in this case does not lead to the development of such event. However, a refined analysis at the smaller pore scale would be necessary to investigate further its possible occurrence.

The experiment at intermediate log(Ca) captures effectively a transition towards capillary fingering. In this case, the capillary and viscous forces become comparable and a competition between the two forces driving the invasion process is seen to influence the aspect of the flow pattern. The increase in pore space saturation shows a stabilization of the invasion front with a transition towards capillary fingering. This stabilization of the front occurs as a result of capillary effects, which slow down the growth of viscous instabilities over short length scales (Daripa and Paşa, 2008; Berg and Ott, 2012). For the low capillary number experiment, observable features of the invading fluid pattern, such as wider and more compact invasion front with increased radial growth, are associated with the capillary fingering dominated regime. The clearly distinguishable contrast in morphology between experiments can be related to the fraction of the resident fluid that has been displaced from the initial pore space volume.

The experimental setup presented in this paper demonstrates the existence of similarities in fluid flow patterns between the investigated natural heterogeneous rock and previously studied 2D porous media. Therefore, the results of this study provides a first insight into the immiscible fluid flow characteristics at the mesoscale in such material and indicates a range of values expected for a transition to occur in the invasion process. It is evident, however, that the bottleneck to further investigate the invasion process in the viscous fingering regime lies in the speed of image acquisition. To extend the analysis to quantitative measurements, a similar experimental method should be used in conjunction with faster x-ray tomography, such as image beamlines at synchrotron facilities. Alternatively, recently developed methods in 3D volumes reconstructions with a limited number of projections could be adapted to enhance the acquisition time resolution.

CONFLICT OF INTEREST STATEMENT

The authors declare that the research was conducted in the absence of any commercial or financial relationships that could be construed as a potential conflict of interest.

AUTHOR CONTRIBUTIONS

All authors listed have made a substantial, direct and intellectual contribution to the work, and approved it for publication.

FUNDING

This work was carried out within the framework of the Stoweng project (ANR-18-CE05-0033). Laboratoire 3SR is part of the LabEx Tec 21 (ANR-11- LABX-0030).

ACKNOWLEDGMENTS

The authors thank Pascal Charrier for his valuable help with the experiments performed in the x-ray scanner at Laboratoire 3SR.

REFERENCES

Berg, S., Oedai, S., and Ott, H. (2013). Displacement and mass transfer between saturated and unsaturated CO2–brine systems in sandstone. *International Journal of Greenhouse Gas Control* 12, 478–492. doi:10.1016/j.ijggc.2011.04.005

Berg, S. and Ott, H. (2012). Stability of CO2–brine immiscible displacement. *International Journal of Greenhouse Gas Control* 11, 188–203. doi:10.1016/j.ijggc.2012.07.001

Brock, D. and Orr, F. (1991). Flow visualization of viscous fingering in heterogeneous porous media. In *SPE Annual Technical Conference and Exhibition* (OnePetro)

Chen, J.-D. and Wilkinson, D. (1985). Pore-Scale Viscous Fingering in Porous Media. *Phys. Rev. Lett.* 55, 1892–1895. doi:10.1103/PhysRevLett.55.1892

Culligan, K., Wildenschild, D., Christensen, B., Gray, W., and Rivers, M. (2006). Pore-scale characteristics of multiphase flow in porous media: A comparison of air–water and oil–water experiments. *Advances in Water Resources* 29, 227–238. doi:10.1016/j.advwatres.2005.03.021

Daripa, P. and Paşa, G. (2008). On Capillary Slowdown of Viscous Fingering in Immiscible Displacement in Porous Media. *Transp Porous Med* 75, 1–16. doi:10.1007/s11242-008-9211-2

Datta, S. S., Chiang, H., Ramakrishnan, T. S., and Weitz, D. A. (2013). Spatial Fluctuations of Fluid Velocities in Flow through a Three-Dimensional Porous Medium. *Phys. Rev. Lett.* 111, 064501. doi:10.1103/PhysRevLett.111.064501

De Wit, A. and Homsy, G. M. (1997). Viscous fingering in periodically heterogeneous porous media. II. Numerical simulations. *The Journal of Chemical Physics* 107, 9619–9628. doi:10.1063/1.475259

Dias, M. M. and Wilkinson, D. (1986). Percolation with trapping. *J. Phys. A: Math. Gen.* 19, 3131–3146. doi:10.1088/0305-4470/19/15/034

Feder, J. (1988). *Fractals* (Boston, MA: Springer US). doi:10.1007/978-1-4899-2124-6

Hele-Shaw, H. S. (1898). Flow of water. *Nature* 58, 520–520

Hu, Y., Patmonoaji, A., Zhang, C., and Suekane, T. (2020). Experimental study on the displacement patterns and the phase diagram of immiscible fluid displacement in three-dimensional porous media. *Advances in Water Resources* 140, 103584. doi:10.1016/j.advwatres.2020.103584

Khosravian, H., Joekar-Niasar, V., and Shokri, N. (2015). Effects of flow history on oil entrapment in porous media: An experimental study. *AIChE J.* 61, 1385–1390. doi:10.1002/aic.14708

Laliberté, M. (2007). Model for Calculating the Viscosity of Aqueous Solutions. *J. Chem. Eng. Data* 52, 321–335. doi:10.1021/je0604075

Lenormand, R., Touboul, E., and Zarcone, C. (1988). Numerical models and experiments on immiscible displacements in porous media. *J. Fluid Mech.* 189, 165–187. doi:10.1017/S0022112088000953

Lenormand, R. and Zarcone, C. (1985). Invasion Percolation in an Etched Network: Measurement of a Fractal Dimension. *Phys. Rev. Lett.* 54, 2226–2229. doi:10.1103/PhysRevLett.54.2226

Liu, H., Zhang, Y., and Valocchi, A. J. (2015). Lattice Boltzmann simulation of immiscible fluid displacement in porous media: Homogeneous versus heterogeneous pore network. *Physics of Fluids* 27, 052103. doi:10.1063/1.4921611

Løvoll, G., Jankov, M., Måløy, K. J., Toussaint, R., Schmittbuhl, J., Schäfer, G., et al. (2011). Influence of Viscous Fingering on Dynamic Saturation–Pressure Curves in Porous Media. *Transp Porous Med* 86, 305–324. doi:10.1007/s11242-010-9622-8

Måløy, K. J., Feder, J., and Jøssang, T. (1985). Viscous Fingering Fractals in Porous Media. *Phys. Rev. Lett.* 55, 2688–2691. doi:10.1103/PhysRevLett.55.2688

Paterson, L. (1981). Radial fingering in a Hele Shaw cell. *Journal of Fluid Mechanics* 113, 513–529

Perrin, J.-C. and Benson, S. (2010). An Experimental Study on the Influence of Sub-Core Scale Heterogeneities on CO2 Distribution in Reservoir Rocks. *Transp Porous Med* 82, 93–109. doi:10.1007/s11242-009-9426-x

Prodanović, M., Lindquist, W., and Seright, R. (2007). 3D image-based characterization of fluid displacement in a Berea core. *Advances in Water Resources* 30, 214–226. doi:10.1016/j.advwatres.2005.05.015

Riaz, A., Tang, G.-Q., Tchelepi, H. A., and Kovscek, A. R. (2007). Forced imbibition in natural porous media: Comparison between experiments and continuum models. *Phys. Rev. E* 75, 036305. doi:10.1103/PhysRevE.75.036305

Rücker, M., Berg, S., Armstrong, R. T., Georgiadis, A., Ott, H., Schwing, A., et al. (2015). From connected pathway flow to ganglion dynamics. *Geophys. Res. Lett.* 42, 3888–3894. doi:10.1002/2015GL064007

Singh, K., Scholl, H., Brinkmann, M., Michiel, M. D., Scheel, M., Herminghaus, S., et al. (2017). The Role of Local Instabilities in Fluid Invasion into Permeable Media. *Sci Rep* 7, 444. doi:10.1038/s41598-017-00191-y

Spurin, C., Bultreys, T., Bijeljic, B., Blunt, M. J., and Krevor, S. (2019). Intermittent fluid connectivity during two-phase flow in a heterogeneous carbonate rock. *Physical Review E* 100, 043103

Stauffer, C. E. (1965). The Measurement of Surface Tension by the Pendant Drop Technique. *J. Phys. Chem.* 69, 1933–1938. doi:10.1021/j100890a024

Toussaint, R., Løvoll, G., Méheust, Y., Måløy, K. J., and Schmittbuhl, J. (2005). Influence of pore-scale disorder on viscous fingering during drainage. *Europhys. Lett.* 71, 583–589. doi:10.1209/epl/i2005-10136-9

Tsuji, T., Jiang, F., and Christensen, K. T. (2016). Characterization of immiscible fluid displacement processes with various capillary numbers and viscosity ratios in 3D natural sandstone. *Advances in Water Resources* 95, 3–15. doi:10.1016/j.advwatres.2016.03.005

Viggiani, G., Andò, E., Takano, D., and Santamarina, J. C. (2014). Laboratory X-ray Tomography: A Valuable Experimental Tool for Revealing Processes in Soils. *Geotech. Test. J.* 38, 20140060. doi:10.1520/GTJ20140060

Zhao, B., MacMinn, C. W., and Juanes, R. (2016). Wettability control on multiphase flow in patterned microfluidics. *Proc Natl Acad Sci USA* 113, 10251–10256. doi:10.1073/pnas.1603387113

FIGURE CAPTIONS

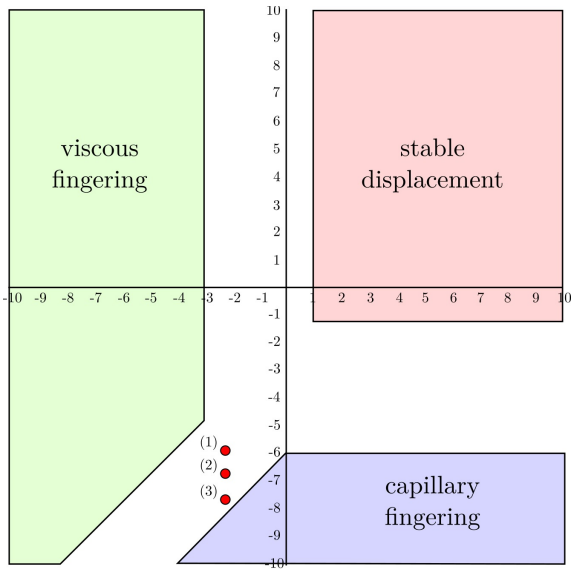

Figure 1. Phase diagram on a log(M)-log(Ca) scale and limits of the three fluid flow regimes. The three experiments at a log(Ca) of -5.90 (1), -6.67 (2) and -7.67 (3) are identified.

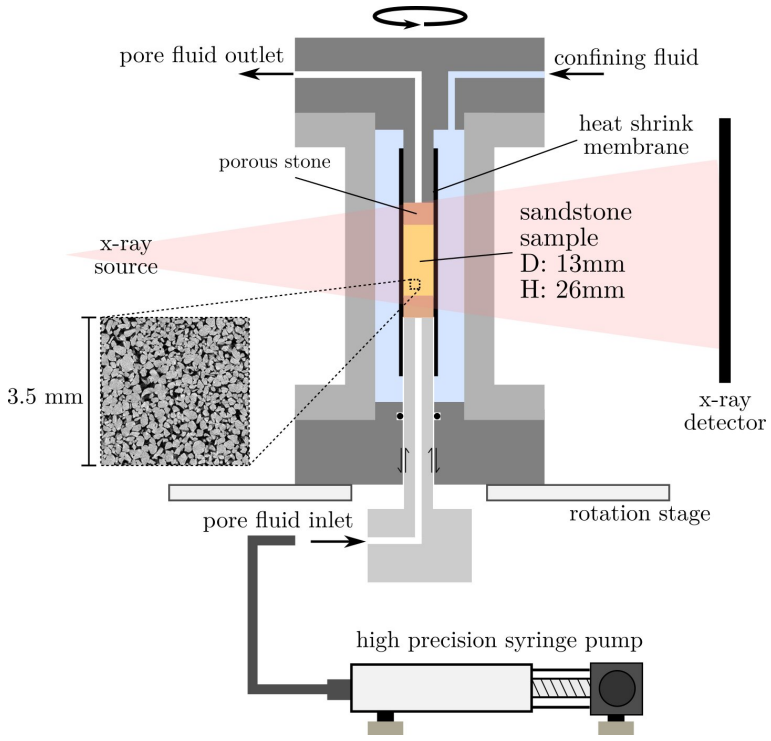

Figure 2. Schematic view of the different components of the fluid injection triaxial system and syringe pump. This configuration enables radiography and tomography imaging of the whole sample. A representative view of the pore structure is shown in the magnified inset.

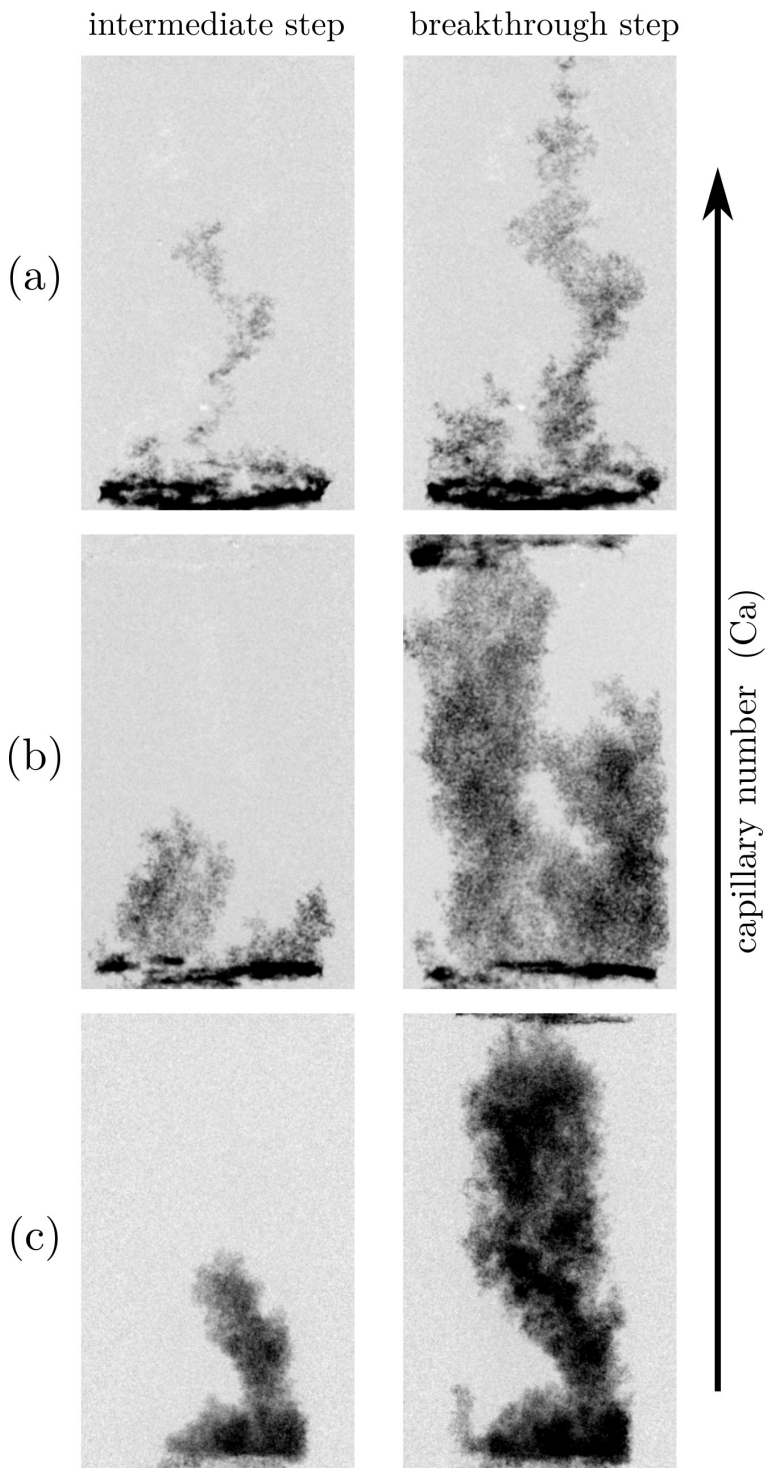

Figure 3. Radiography representation of finger patterns at an intermediate and breakthrough step during injection of the invading (water) and defending (oil) fluids. Experiments at three capillary numbers: log(Ca)=-5.90 (a) log(Ca)=-6.67 (b) and log(Ca)=-7.67 (c).

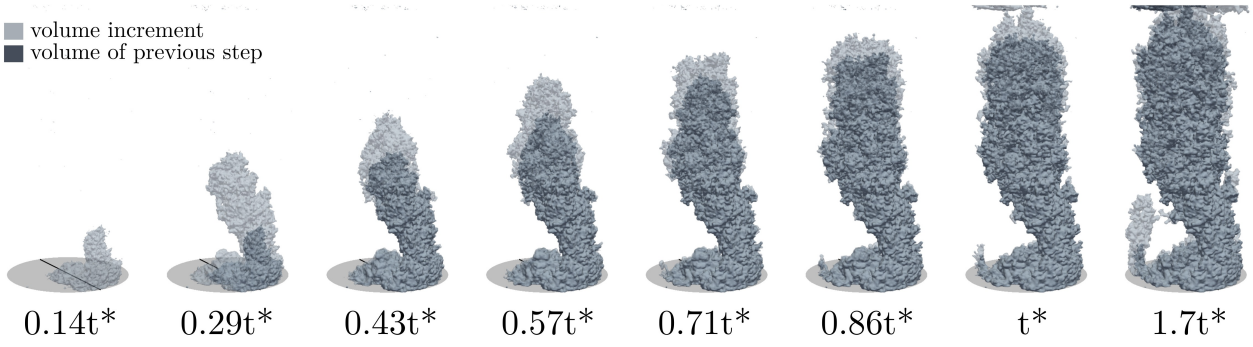

Figure 4. X-ray tomography reconstruction of the finger pattern for a low capillary number (Ca=-7.67, same as Figure 3c). The slow process enables to capture the development of capillary fingering in 3D.